Air Force Institute of Technology
AFIT Scholar

Faculty Publications

12-1-2019

Generating Electromagnetic Nonuniformly Correlated Beams

Milo W. Hyde IV
Air Force Institute of Technology

Xifeng Xiao

David G. Voelz
New Mexico State University

Follow this and additional works at: https://scholar.afit.edu/facpub

 Part of the Electromagnetics and Photonics Commons, and the Plasma and Beam Physics Commons

Recommended Citation

Hyde, M. W., Xiao, X., & Voelz, D. G. D. G. (2019). Generating electromagnetic nonuniformly correlated beams. Optics Letters, 44(23), 5719–5722. https://doi.org/10.1364/OL.44.005719

This Article is brought to you for free and open access by AFIT Scholar. It has been accepted for inclusion in Faculty Publications by an authorized administrator of AFIT Scholar. For more information, please contact richard.mansfield@afit.edu.

Optics Letters

Generating electromagnetic nonuniformly correlated beams

Milo W. Hyde IV,[1,*] Xifeng Xiao,[2] and David G. Voelz[3]

[1]Air Force Institute of Technology, Dayton, Ohio 45433, USA
[2]Ball Aerospace & Technologies Corp., Albuquerque, New Mexico 87106, USA
[3]New Mexico State University, Las Cruces, New Mexico 88003, USA
*Corresponding author: milo.hyde@us.af.mil

Received 26 September 2019; revised 27 October 2019; accepted 28 October 2019; posted 28 October 2019 (Doc. ID 378851); published 25 November 2019

We develop a method to generate electromagnetic nonuniformly correlated (ENUC) sources from vector Gaussian Schell-model (GSM) beams. Having spatially varying correlation properties, ENUC sources are more difficult to synthesize than their Schell-model counterparts (which can be generated by filtering circular complex Gaussian random numbers) and, in past work, have only been realized using Cholesky decomposition—a computationally intensive procedure. Here we transform electromagnetic GSM field instances directly into ENUC instances, thereby avoiding computing Cholesky factors resulting in significant savings in time and computing resources. We validate our method by generating (via simulation) an ENUC beam with desired parameters. We find the simulated results to be in excellent agreement with the theoretical predictions. This new method for generating ENUC sources can be directly implemented on existing spatial-light-modulator-based vector beam generators and will be useful in applications where nonuniformly correlated beams have shown promise, e.g., free-space/underwater optical communications. © 2019 Optical Society of America

https://doi.org/10.1364/OL.44.005719

Provided under the terms of the OSA Open Access Publishing Agreement

Compared to uniformly correlated or Schell-model partially coherent sources, nonuniformly correlated (NUC) sources are a relatively recent and lightly researched subject. NUC sources have spatially varying correlation properties, giving them fascinating propagation or beam characteristics beyond those of Schell-model sources. Originally introduced by Lajunen and Saastamoinen in 2011 [1] and generalized (vectorized) shortly thereafter [2], NUC sources have since been shown to outperform—in terms of the first and second moments of intensity—both coherent Gaussian and Gaussian Schell-model (GSM) beams when propagated through turbulent media [3].

This has motivated more recent work in synthesizing NUC beams for use in applications such as free-space/underwater optical communications [4–7]. Because of their spatially varying correlation properties, NUC sources are inherently more difficult to generate than uniformly correlated sources. Nearly all of the existing NUC synthesis literature concerns scalar NUC sources and, generally, those techniques cannot be applied to synthesize vector or electromagnetic nonuniformly correlated (ENUC) beams. Only one Letter (Ref. [7]) known to the authors has synthesized ENUC sources, and the results were limited for two main reasons: (1) the ENUC field realizations were synthesized using Cholesky decomposition—a computationally onerous procedure in terms of both memory and processing power, and (2) there was limited control over the cross-polarization correlation functions (W_{xy} and W_{yx}) of the resulting ENUC cross-spectral density (CSD) matrix $\underline{\mathbf{W}}$.

In this Letter, we address both of these limitations and successfully demonstrate how to generate ENUC beams using a spatial-light-modulator (SLM)-based system such as that described in Ref. [7]. We start by presenting how to transform GSM field instances into NUC instances with a simple nonlinear transform [8]. GSM beams, being uniformly correlated, can be synthesized by filtering circular complex Gaussian random numbers (CCGRNs) [9]. The filtering is typically performed in the frequency domain using fast Fourier transforms (FFTs). Being able to take GSM field instances and transform them into NUC realizations, thereby avoiding computing Cholesky factors, is the main contribution of this Letter.

Next, we show how to control W_{xy} and W_{yx} by adapting a recently published technique designed specifically for Schell-model sources [10]. From this analysis, we find the range of physically synthesizable, as opposed to physically realizable [2], ENUC sources. Lastly, we present the simulation results where we generate an ENUC source with desired parameters. We compare the simulated results to the theoretical predictions to validate our method. We conclude with a brief summary of this Letter and a list of potential applications.

We begin with the CSD matrix $\underline{\mathbf{W}}$ of an ENUC source [2]:

$$W_{\alpha\beta}(\boldsymbol{\rho}_1,\boldsymbol{\rho}_2) = A_\alpha \exp\left(-\frac{\rho_1^2}{4\sigma_\alpha^2}\right) A_\beta \exp\left(-\frac{\rho_2^2}{4\sigma_\beta^2}\right) \times B_{\alpha\beta} \exp[-(|\boldsymbol{\rho}_1-\boldsymbol{\gamma}_\alpha|^2-|\boldsymbol{\rho}_2-\boldsymbol{\gamma}_\beta|^2)^2/\delta_{\alpha\beta}^4], \tag{1}$$

where $\alpha = x, y$, $\boldsymbol{\rho} = \hat{\mathbf{x}}x + \hat{\mathbf{y}}y$, and A_α and σ_α are the amplitude and rms width of the α field component, respectively. Also in

Eq. (1), $\delta_{\alpha\beta}$ is the cross-correlation width, $B_{\alpha\beta}$ is the complex cross-correlation coefficient, and $\boldsymbol{\gamma}_\alpha$ is a real two-dimensional (2D) vector that shifts the maximum of the correlation function away from the origin.

We desire to generate ENUC stochastic field realizations of the form

$$\boldsymbol{E}(\boldsymbol{\rho}) = \hat{\boldsymbol{x}}E_x(\boldsymbol{\rho}) + \hat{\boldsymbol{y}}E_y(\boldsymbol{\rho})$$
$$E_\alpha(\boldsymbol{\rho}) = C_\alpha \exp\left(-\frac{\rho^2}{4\sigma_\alpha^2}\right) T_\alpha(\boldsymbol{\rho}), \tag{2}$$

where C_α is a complex constant, and T_α is a complex screen generated from correlated complex Gaussian random numbers. Taking the vector auto-correlation of Eq. (2) and comparing the resulting expression to Eq. (1), we see at once that $A_\alpha = |C_\alpha|$, $\arg(C_x C_y^*) = \arg(B_{xy})$, and

$$\langle T_\alpha(\boldsymbol{\rho}_1) T_\beta^*(\boldsymbol{\rho}_2)\rangle = |B_{\alpha\beta}| \exp[-(|\boldsymbol{\rho}_1 - \boldsymbol{\gamma}_\alpha|^2 - |\boldsymbol{\rho}_2 - \boldsymbol{\gamma}_\beta|^2)^2/\delta_{\alpha\beta}^4]. \tag{3}$$

Thus, we can generate ENUC field instances by producing two screens with the second-order moments given in Eq. (3) and then applying Eq. (2).

We note that T_x and T_y are statistically inhomogeneous and, therefore, difficult to synthesize. In Ref. [7], T_x and T_y were generated using a Cholesky factorization, which is computationally prohibitive, i.e., $O(n^3)$ complexity to compute the Cholesky factor and then $O(n^2)$ (matrix-vector products) to synthesize T_x and T_y. For example, assume that the desired T_x and T_y are 512×512 grids, which is a common size for commercially available SLMs. The covariance matrix in Eq. (3) would be a staggering $2^{20} \times 2^{20}$ matrix, which would require a supercomputer to store and compute the Cholesky factors. In Ref. [7], the authors generated T_x and T_y on much smaller grids and then interpolated the screens to 512×512.

Considering the above example, it clearly would be beneficial to have another method to generate ENUC screens other than Cholesky decomposition. Here we propose to transform electromagnetic Gaussian Schell-model (EGSM) screens, which are statistically homogeneous and can be generated by filtering CCGRNs [9], directly into ENUC screens. To do so, we begin by expressing the EGSM $\underline{\mathbf{W}}$ as [11]

$$W_{\alpha\beta}(\boldsymbol{\rho}_1, \boldsymbol{\rho}_2) = A_\alpha \exp\left(-\frac{\rho_1^2}{4\sigma_\alpha^2}\right) A_\beta \exp\left(-\frac{\rho_2^2}{4\sigma_\beta^2}\right) \times B_{\alpha\beta} \exp(-|\boldsymbol{r}_1 - \boldsymbol{r}_2|^2/\delta_{\alpha\beta}^4). \tag{4}$$

This differs from the traditional EGSM $\underline{\mathbf{W}}$ in regard to the power of $\delta_{\alpha\beta}$, which is typically squared. Here we raise it to the fourth power to match the ENUC correlation function. We have also introduced $\boldsymbol{r}$, which is a vector function of $\boldsymbol{\rho}$, in the EGSM correlation function for ultimately the same reason.

Comparing the correlation functions in Eqs. (1) and (4), we see at once that

$$\boldsymbol{r} = \hat{\boldsymbol{\alpha}}|\boldsymbol{\rho} - \boldsymbol{\gamma}|^2. \tag{5}$$

This quite simply means that we can generate an ENUC T_α by mapping the EGSM T_α values at $\boldsymbol{r}$ to $\boldsymbol{\rho}$ via Eq. (5). We also note that because of Eq. (5), the ENUC T_α are rotationally symmetric about $\boldsymbol{\gamma}$.

The proposed ENUC screen generation process is best illustrated by example. Here we wish to generate an ENUC T_α with $\delta_{\alpha\alpha}$, σ_α, and $\boldsymbol{\gamma}_\alpha$—we will generalize this to produce a full ENUC source later in the Letter. We start by determining the size of the grid in $\boldsymbol{\rho}$ space. This grid must be large enough to "fit" the ENUC $W_{\alpha\alpha}$. To keep things general, we assume that $\boldsymbol{\rho} \in [-L/2, L/2]$. Equation (5) maps $\boldsymbol{\rho}$ into $\boldsymbol{r}$ space such that $\boldsymbol{r} \in [0, (\sqrt{2}L/2 + |\boldsymbol{\gamma}_\alpha|)^2]$, where the $\sqrt{2}$ comes from considering the square $\boldsymbol{\rho}$ grid at its maximum distance from the origin.

Now that we have the grid size in the $\boldsymbol{r}$ plane, we need to determine the grid spacing Δ. This spacing should be fine enough to capture the variation of T_α in $\boldsymbol{r}$ space, which is related to $\delta_{\alpha\alpha}$. The required Δ has been discussed in many past Letters, and $\Delta \le \delta_{\alpha\alpha}/5$ is sufficient [9]. The number of grid points is $N = \lceil(\sqrt{2}L/2 + |\boldsymbol{\gamma}_\alpha|)^2/\Delta\rceil$.

The next step is to generate an EGSM T_α. This process has been described in the literature many times [7,9,11]. Here we provide the final result for the reader's convenience:

$$T_\alpha[i,j] = \sum_{m,n} r_\alpha[m,n] \sqrt{\frac{\Phi_{\alpha\alpha}[m,n]}{2(N\Delta)^2}} \exp\left[\mathrm{j}\frac{2\pi}{N}(mi + nj)\right], \tag{6}$$

where i,j are the discrete spatial indices in the $\boldsymbol{r}$ plane ($\xi = i\Delta, \eta = j\Delta$), m, n are discrete spatial frequency indices, and r_α is an $N \times N$ matrix of zero-mean, unit-variance, CCGRNs. Also in Eq. (6), $\Phi_{\alpha\alpha}$ is the spatial power spectrum—the Fourier transform of the EGSM correlation function in Eq. (4)—and equal to

$$\Phi_{\alpha\alpha}(\boldsymbol{f}) = \pi\delta_{\alpha\alpha}^4 \exp(-\pi^2\delta_{\alpha\alpha}^4 f^2). \tag{7}$$

Here $\boldsymbol{f} = \hat{\boldsymbol{x}}f_x + \hat{\boldsymbol{y}}f_y$ is the continuous spatial frequency coordinate and related to m, n by $f_x = m/(N\Delta)$, $f_y = n/(N\Delta)$. Figure 1(a) shows an example of the real part of T_α generated by evaluating Eq. (6) using FFTs.

Recall that $\boldsymbol{r} \in [0, (\sqrt{2}L/2 + |\boldsymbol{\gamma}_\alpha|)^2]$, and, therefore, we only need a single "radial slice" of an EGSM T_α to produce an ENUC T_α. An example of this is shown in Fig. 1(b), which is the radial slice along the ξ axis of the T_α in Fig. 1(a).

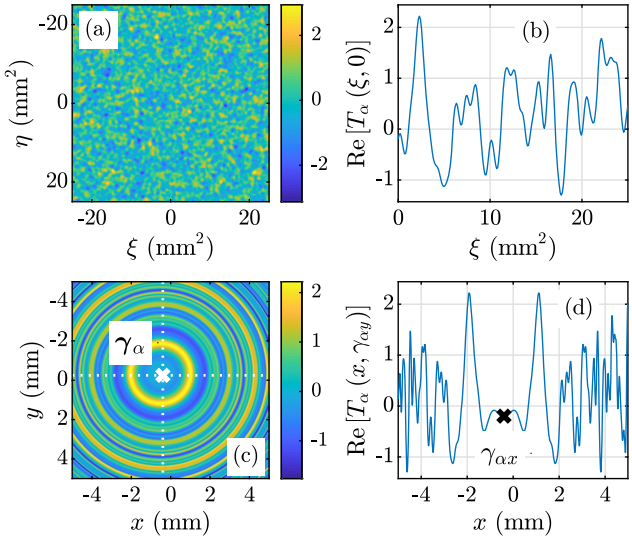

Fig. 1. ENUC T_α generation process. (a) Real part of an EGSM T_α on the $\boldsymbol{r} = \hat{\boldsymbol{x}}\xi + \hat{\boldsymbol{y}}\eta$ grid, (b) radial slice along ξ axis of the EGSM T_α in (a), (c) real part of ENUC T_α formed from mapping the T_α values in (b) to $\boldsymbol{\rho}$ using Eq. (5), and (d) $y = \gamma_{\alpha y}$ slice through (c).

Lastly, we map the T_α values at $\boldsymbol{r}$ to $\boldsymbol{\rho}$ using Eq. (5). This will likely require interpolation, especially if the points in the $\boldsymbol{\rho}$ grid—such as those in the $\boldsymbol{r}$ grid—are uniformly spaced (as is often the case). Figure 1(c) shows the end result of this process, and the real part of the ENUC T_α formed from the EGSM T_α in Fig. 1(a).

The ENUC screen [Fig. 1(c)] is rotationally symmetric about the point $\boldsymbol{\gamma}_\alpha$. Examining Figs. 1(b)–1(d), one can clearly see the effects of the mapping from $\boldsymbol{r}$ to $\boldsymbol{\rho}$: the screen features near $\xi = 0$ in (b) map to locations near $\boldsymbol{\gamma}_\alpha$ in (c). These features are clearly evident in (d), which shows the $y = \gamma_{\alpha y}$ slice through (c). As a result of the quadratic transformation in Eq. (5), the features near $\xi = 0$ in (b) are spatially elongated or stretched [see the region around $x = \gamma_{\alpha x}$ in (d)]. As we move away from $\xi = 0$, the screen features transition from being stretched to compressed, again due to the quadratic mapping in Eq. (5).

The procedure in the preceding paragraphs controls the "self" or diagonal elements of the ENUC $\underline{\underline{\mathbf{W}}}$ and, therefore, is sufficient to generate ENUC beams that are linearly and partially polarized. To generate ENUC beams that are circularly or more generally, elliptically polarized, we must precisely control the off-diagonal elements of the ENUC $\underline{\underline{\mathbf{W}}}$, namely, W_{xy} and W_{yx}.

In Ref. [10], the author controls the full $\underline{\underline{\mathbf{W}}}$ of electromagnetic Schell-model sources by using a spatially varying, complex, cross-correlation coefficient R between the random numbers (r_x and r_y) that seed T_x and T_y. Specialized to the problem here, R takes the form

$$R(\boldsymbol{f}) = \frac{\delta_{xy}^4}{\delta_{xx}^2\delta_{yy}^2/|B_{xy}|}\exp\left[-\pi^2\left(\delta_{xy}^4 - \frac{\delta_{xx}^4+\delta_{yy}^4}{2}\right)f^2\right], \tag{8}$$

where $R \in [-1, 1]\,\forall \boldsymbol{f}$. This stipulation on R is an obvious mathematical condition and is closely related to the physical realizability criteria of EGSM and by Eq. (5), ENUC sources [2,11]. For convenience, we let $R = Cg$, where C and g represent the coefficient and exponential function in Eq. (8), respectively.

It is important to check, using the realizability criteria, that indeed $R \in [-1, 1]\,\forall \boldsymbol{f}$. Since we are ultimately interested in producing ENUC sources, we must use the ENUC realizability criteria [2]:

$$B_{\alpha\alpha} = 1, B_{xy} = B_{yx}^*, |B_{xy}| \le 1, \delta_{xy} = \delta_{yx},$$
$$\times\sqrt[4]{\frac{\delta_{xx}^4+\delta_{yy}^4}{2}} \le \delta_{xy} \le \sqrt{\frac{\delta_{xx}\delta_{yy}}{|B_{xy}|}}. \tag{9}$$

We focus on the fork inequality on the second line of Eq. (9). At the inequality's lower limit, $g = 1$ and $C < 1$, meaning that $R \in [-1, 1]$. At the upper limit, $0 < g \le 1$ and $C = 1/|B_{xy}|$. Since $|B_{xy}| \le 1$, C is generally inconsistent with $R \in [-1, 1]\,\forall \boldsymbol{f}$. Thus, the approach for generating ENUC beams presented here cannot produce all physically realizable ENUC sources.

This raises the question: what ENUC δ_{xy} and $|B_{xy}|$ can the technique produce, or, more fundamentally, what are the technique's synthesizability criteria or limits? Recall that $R \in [-1, 1]$ at the lower limit of the fork inequality in Eq. (9). Therefore, this δ_{xy} value sets the lower synthesizability limit. At the upper synthesizability limit, $C \le 1$. Using the expression for C in Eq. (8) and some simple algebra, it is easy to show that

$$\sqrt[4]{\frac{\delta_{xx}^4+\delta_{yy}^4}{2}} \le \delta_{xy} \le \sqrt{\frac{\delta_{xx}\delta_{yy}}{|B_{xy}|}} \tag{10}$$

for $R \in [-1, 1]\,\forall \boldsymbol{f}$. The fork inequality in Eq. (10) and the first line of Eq. (9) constitute the synthesizability criteria.

To show how Eq. (10) differs from Eq. (9), we set $\delta_{xx} = \delta_{yy} = \delta$ and plot both inequalities versus $|B_{xy}|$ in Fig. 2. The solid black curve demarks the maximum physically allowed values of $\delta_{xy}/\delta - 1$ and corresponds to the upper limit in Eq. (9). The values of $\delta_{xy}/\delta - 1$ above this curve (the solid red region in the figure) are not physically realizable. The dashed black curve denotes the maximum synthesizable values of $\delta_{xy}/\delta - 1$ and corresponds to the upper limit in Eq. (10). The area below this curve (shaded in green) is the synthesizable region. Between the curves, shaded in yellow, is the region that is physically realizable, but not synthesizable. Although physically permitted, the values of $\delta_{xy}/\delta - 1$ in this region cannot be generated using the technique presented here. For general δ_{xx} and δ_{yy}, the synthesizable region is always inside the realizability volume and, therefore, for a given δ_{xx}, δ_{yy}, and $|B_{xy}|$, $\max(\delta_{xy}^{\text{real}}) \ge \max(\delta_{xy}^{\text{synth}})$.

Having derived the synthesizability criteria and having discussed how to generate ENUC T_x and T_y from the corresponding EGSM screens, we now present the simulation results where we synthesize an ENUC source with the parameters listed in Table 1. Note that we chose these values for proof-of-concept purposes only. When designing an ENUC beam for use in a specific application, it is imperative to understand how these parameters affect the beam shape, coherence, and polarization of the propagating ENUC beam. This analysis is presented in Refs. [2,11] and is not included here for brevity. Before presenting the simulation results, we briefly discuss the setup.

As we show in Code 1, Ref. [12], we used grids with $N = 1024$ points per side and side lengths $L = 10$ mm. The grid spacing in $\boldsymbol{\rho}$ space was $L/N = 9.77$ μm. These numbers,

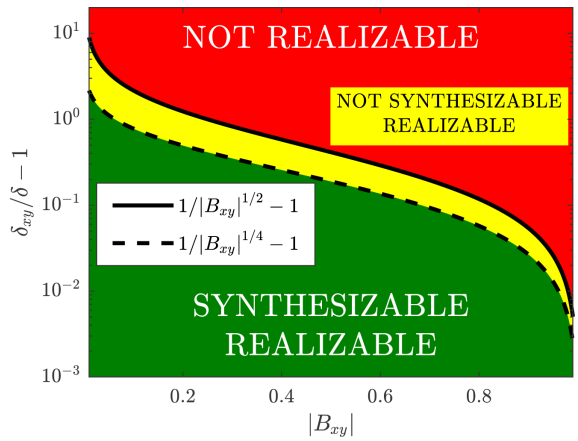

Fig. 2. ENUC physical realizability [Eq. (9)] versus synthesizability [Eq. (10)] for $\delta_{xx} = \delta_{yy} = \delta$.

Table 1. ENUC Parameters

A_x	1	σ_x	1.1 mm	δ_{xx}	0.8 mm
A_y	1.2	σ_y	1.0 mm	δ_{yy}	0.7 mm
B_{xy}	$0.4\exp(-j\pi/6)$			δ_{xy}	0.763 mm
$\boldsymbol{\gamma}_x$	$\hat{\mathbf{x}}0.35 + \hat{\mathbf{y}}0.5$ mm			$\boldsymbol{\gamma}_y$	$-\hat{\mathbf{x}}0.4 - \hat{\mathbf{y}}0.25$ mm

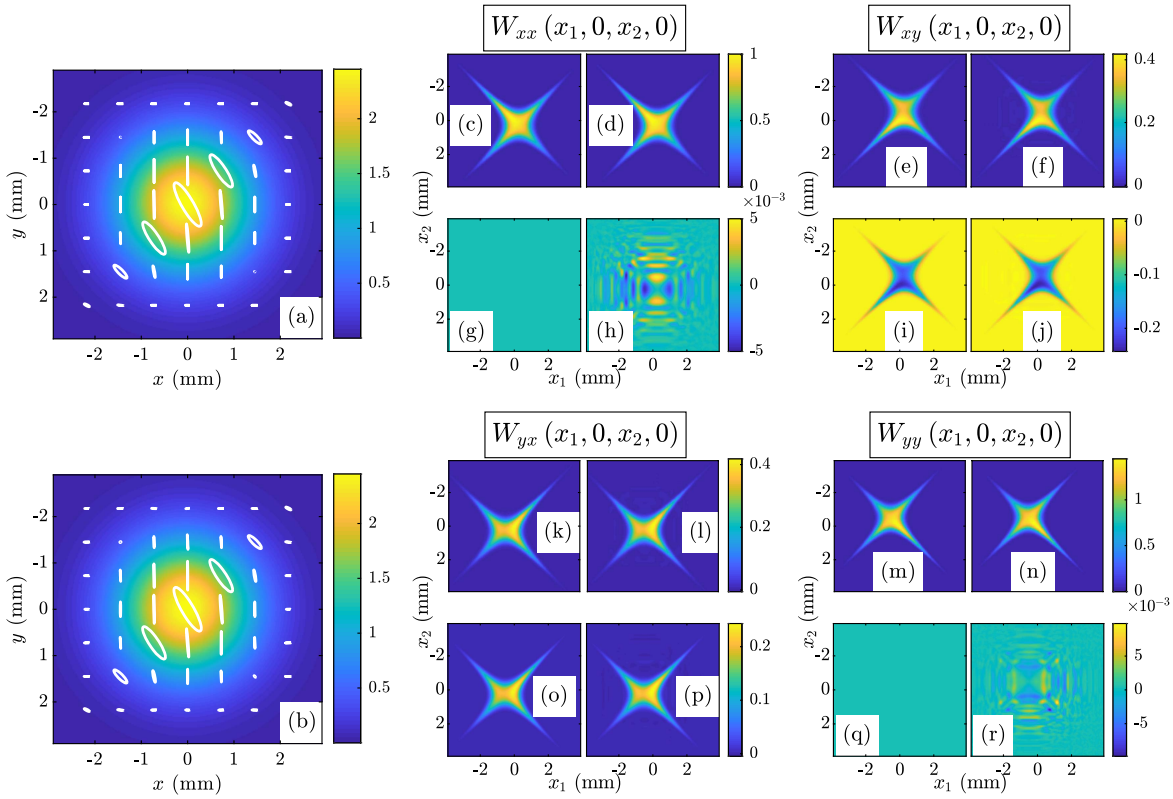

Fig. 3. ENUC simulation results: subfigures (a) and (b) show the theoretical and simulated spectral densities overlaid with the polarization ellipses. Subfigures (c)–(r) show the elements of $\underline{\mathbf{W}}(x_1, 0, x_2, 0)$. Each element (labeled for the reader's convenience) is a 2×2 group of images, where the theoretical and simulated $W_{\alpha\beta}$ are in columns 1 and 2 and the real and imaginary parts of $W_{\alpha\beta}$ are in rows 1 and 2, respectively.

combined with the $\boldsymbol{\gamma}_x$ and $\boldsymbol{\gamma}_y$ in Table 1, corresponded to a "side length" in $\boldsymbol{r}$ space of 118.0077 mm^2 and a spacing of $\Delta = 0.1152$ mm^2.

We generated correlated EGSM T_x and T_y using Table 1 and Eqs. (6)–(8). We then transformed those EGSM screens to ENUC screens following the procedure described above and shown pictorially in Fig. 1. We lastly produced an ENUC field instance using Eq. (2).

We used 50,000 ENUC field realizations to compute the spectral density, polarization ellipses, and $\underline{\mathbf{W}}(x_1, 0, x_2, 0)$. These results are shown in Fig. 3. Overall, the agreement between the simulation and theory is excellent. Note that the visually conspicuous differences between the theoretical and simulated $\mathrm{Im}(W_{xx})$ [Figs. 3(g) and 3(h)] and $\mathrm{Im}(W_{yy})$ [Figs. 3(q) and 3(r)], in fact, are quantitatively small. The color scales of those results are $[-0.005, 0.005]$ and $[-0.0098, 0.0098]$, which are approximately 200 and 150 times smaller than the corresponding real part results.

In summary, we presented a method to generate ENUC beams from EGSM sources. Previous work used Cholesky decomposition—a computationally expensive process—to synthesize ENUC beams [7]. Here we transformed EGSM field instances (generated by filtering CCGRNs) directly into ENUC realizations (without computing Cholesky factors), saving significant computing time and resources. We simulated the generation of an ENUC source with specified parameters. The simulated results were in excellent agreement with the theory, thus validating our approach.

The method for generating ENUC beams presented in this Letter can be directly implemented on existing SLM-based vector beam generators and can be used in any application that utilizes ENUC beams such as free-space or underwater optical communications.

Disclosures. The authors declare no conflicts of interest. The views expressed in this Letter are those of the authors and do not reflect the official policy or position of the U.S. Air Force, the Department of Defense, or the U.S. Government.

REFERENCES

1. H. Lajunen and T. Saastamoinen, Opt. Lett. **36**, 4104 (2011).
2. Z. Tong and O. Korotkova, J. Opt. Soc. Am. A **29**, 2154 (2012).
3. Y. Gu and G. Gbur, Opt. Lett. **38**, 1395 (2013).
4. M. W. Hyde, S. R. Bose-Pillai, and R. A. Wood, Appl. Phys. Lett. **111**, 101106 (2017).
5. M. Santarsiero, R. Martínez-Herrero, D. Maluenda, J. C. G. de Sande, G. Piquero, and F. Gori, Opt. Lett. **42**, 4115 (2017).
6. S. Cui, Z. Chen, L. Zhang, and J. Pu, Opt. Lett. **38**, 4821 (2013).
7. M. W. Hyde, S. Bose-Pillai, D. G. Voelz, and X. Xiao, Phys. Rev. Appl. **6**, 064030 (2016).
8. X. Xiao and D. Voelz, *Imaging and Applied Optics 2017 (3D, AIO, COSI, IS, MATH, pcAOP)*, OSA Technical Digest (online) (OSA, 2017), paper PTu1D.3.
9. D. Voelz, X. Xiao, and O. Korotkova, Opt. Lett. **40**, 352 (2015).
10. M. W. Hyde, Results Phys. **15**, 102663 (2019).
11. O. Korotkova, *Random Light Beams: Theory and Applications* (CRC Press, 2014).
12. M. Hyde, "MATLAB R2018b ENUC simulation code," figshare, 2019, https://doi.org/10.6084/m9.figshare.9901724.

129.92.250.41 {ts '2021-08-06 15:30:28'}